International Journal of Nanomedicine

Dovepress
open access to scientific and medical research

Open Access Full Text Article

ORIGINAL RESEARCH

A carbohydrate mimetic peptide modified size-shrinkable micelle nanocluster for anti-tumor targeting and penetrating drug delivery

This article was published in the following Dove Press journal:
International Journal of Nanomedicine

Qinyue Chen[1]
Huihui Liang[1]
Yali Sun[1]
Yiting Chen[1]
Wenxiu He[1]
Xiaoling Fang[1]
Xianyi Sha[1]
Jinming Li[2]

[1]Department of Pharmaceutics, Key Laboratory of Smart Drug Delivery, Ministry of Education, School of Pharmacy, Fudan University, Shanghai, 201203, People's Republic of China; [2]Department of Colorectal Surgery, Xinhua Hospital, Shanghai Jiaotong University School of Medicine, Shanghai 200092, People's Republic of China

Purpose: To deliver the chemotherapeutics through the nanoparticles, the delivery system should accumulate at the tumor site first and then penetrate through the interstitium into the interior. The specific tumor-targeting pathway mediated via the receptor-ligand binding could achieve the desirable accumulation of nanoparticles, and the nanoparticles with smaller sizes were required for penetration.

Methods and materials: We constructed a size-shrinkable nanocluster modified with a tumor-targeting motif IF-7 (IF-7-MNC) based on a pH-sensitive framework which could be disintegrated in an acid environment to release the micelles aggregated inside. The micelles were constructed by amphiphilic block copolymers PEG–PLA to encapsulate paclitaxel (PTX), while the cross-linked framework consisting of TPGS-PEI was used as a net to gather and release micelles. This nanoplatform could specifically bind with the tumor receptor Annexin A1 through the ligand IF-7 and then shrunk into small micelles with a desirable size for penetration.

Conclusion: IF-7-MNC of 112.27±6.81 nm could shrink into micelles in PBS (0.01 M, pH 5.0) with sizes of 14.89±0.32 nm. The cellular-uptake results showed that IF-7-MNC could be significantly internalized by A549 cells and HUVEC cells, while the penetration of IF-7-MNC could be more prominent into the 3D-tumor spheroids compared with that of MNC. The biodistribution results displayed that the fluorescence of IF-7-MNC in the tumor site at 24 hrs was 4.5-fold stronger than that of MNC. The results of anti-tumor growth demonstrated that IF-7-MNC was more favorable for the tumor therapy than MNC, where the inhibitory rate of tumor growth was 88.29% in the PTX-loaded IF-7-MNC (IF-7-PMNC) treated group, significantly greater than PMNC treatment group ($p<0.05$).

Keywords: nanocluster, IF-7, Annexin A1, tumor targeting, size-shrinkable

Correspondence: Xianyi Sha
Key Laboratory of Smart Drug Delivery, Ministry of Education, School of Pharmacy, Fudan University, 826 Zhangheng Road, Shanghai 201203, People's Republic of China
Tel +86 215 198 0072
Fax +86 215 198 0072
Email shaxy@fudan.edu.cn

Jinming Li
Department of Colorectal Surgery, Xinhua Hospital, Shanghai Jiaotong University School of Medicine, 1665 Kongjiang Road, Shanghai 200092, People's Republic of China
Tel +86 212 507 7855
Email lijinming@xinhuamed.com.cn

Introduction

During the past decades, many clinical therapies have been explored to treat cancers, where chemotherapy, radiotherapy, photothermal therapy, immunotherapy, and targeted therapies like antibody-based approaches are included.[1–4] All these different treatments can be conducted alone or in combination, whereas the efficiency of elongating the life span of patients through methods above is limited;[5,6] and the most widely used therapies, such as chemotherapy, might come along with systematic toxicity affecting the life quality of patients.[7] Accordingly, more accurate and safer therapies for cancer treatment are in demand to improve the survival time as well as the living quality of patients.

To improve the in vivo curative efficacy of chemotherapeutics, researchers have designed several nanovesicles for the drug delivery,[8] among which the micelle is one of the promising types.[9] Known as self-assembled nanoscale particles, the micelle is composited with a hydrophobic core and a hydrophilic shell,[10] allowing it to encapsulate the insoluble drug into the inner side and reduce the uptake by the reticuloendothelial system (RES).[11] However, as a drug delivery nanoplatform, the non-targeting micelle has not displayed very desirable in vivo manner. It has been reported that the paclitaxel (PTX) loaded micelles (PM) showed a short retention in the blood circulation and a similar biodistribution result with Taxol,[12] with only 20% of the micelles found integrated in the blood after 1 hr post-administration.[13] These results indicated that micelles exhibited no significant tumor-targeting ability, while the PEG−PLA just functioned as a solubilizer for hydrophobic chemotherapeutics and could not remain as a nanosized vesicle in the blood.[14] There are also researchers using other natural polymeric materials like some laurylcarbamate derivative to form micellar structures, enhancing the stability of in vivo drug delivery process.[15] Therefore, it is important for the in vivo application of micelles to enhance the accumulation of drug encapsulated in the micelles at the tumor sites as well as minimize the biodistribution in other healthy tissues.

It has long been acknowledged that the physiological traits, including high vascular density and large gaps between endothelial cells,[16] of the solid tumor make it possible for the nanosized particles to retain and penetrate into the tumor sites, which is also known as EPR effect;[17,18] and the favorable particle size for achieving the EPR effect is reported as approximate 100 nm.[19] Nevertheless, some doubts over the EPR effects have risen in recent years. Researchers wondered the actual effectiveness of the particle accumulation in a solid tumor via EPR effect, and clinical outcomes from different nanosized drug delivery systems drug carriers have indicated that EPR is not as reliable as previously thought since the drug-loaded nanocarriers generally failed to exhibit superior efficacy to free drug when studied in clinical trials,[20] which meant that the tumor-targeting efficacy of nanosized particles through EPR effects might be quite limited or in vain.[21,22] Moreover, even when the nanoparticles reached at the periphery of the solid tumor, the fibrillar collagen network would hinder the particles larger than 60 nm from penetrating into the tumor interior site,[23] which conversely indicated that the micelles which were smaller than 15 nm could be the favorable ones to penetrate through the interstitium.

Inspired by the mechanisms above, we previously designed a size-shrinkable micelle nanoclusters (MNC) at ~100 nm based on a TPGS-PEI cross-linked framework which was pH-sensitive and gather micelles inside together.[24] MNC was proved to accumulate at the tumor fringe through EPR effects, swell and disintegrate in the lysosomes which are acidic after being taken into the peripheral cancer cells, and then release the nanosized micelles from the framework for further penetration. Nevertheless, since EPR effects have been found not so prominent in tumor targeting, herein we modified the nanoclusters with a polypeptide IF-7 to improve the targeting efficiency of MNC through the receptor-mediated active targeting strategies.

As synthetic amino acids with seven short peptides (IFLLWQR), IF-7 is an analog of AnnA1 IgG, which could specifically bind to the 15 KDa fragment of Annexin A1.[25] Annexin A1, also known as AnnA1, is a member of a superfamily of annexin proteins and binds to acidic phospholipids in the presence of Ca^{2+}.[26] Researches have studied its various functions in the tumor progress: Cheng et al, found that AnnA1 was highly expressed in the gastric cancer and related with the invasiveness of tumor cells;[27] and Marjo de Graauw et al, found it facilitated the breast cancer cells to colonize at the distant organs.[28] In addition, the expression of AnnA1 was also found in vascular endothelial cells of the solid tumor, whose expression was significantly higher than that of vascular endothelial growth factor receptor, making it a potential target for efficient utilization in receptor-ligand binding.[29,30]

In this study, combined the active targeting strategy mediated by receptor-ligand binding with the size-shrinkable characteristics through the pH-sensitive framework, we designed IF-7 modified size-shrinkable nanoclusters (IF-7-MNC) to achieve the enhanced tumor targeting and penetration. The in vitro and in vivo evaluations have been carried out to prove the targeting efficacy and size-shrinkable efficacy in the acid environment of IF-7-MNC (Scheme 1).

Materials and methods

Materials

PEG2000-PLA2000 was purchased from JenKem Technology Co., Ltd. (Beijing, China). TPGS was purchased from Eastman Chemical (Kingsport; TN, USA). PTX was from Jiangsu Yew Pharmaceutical Co., Ltd. (Wuxi, China). IgG was from Shanghai Rongsheng

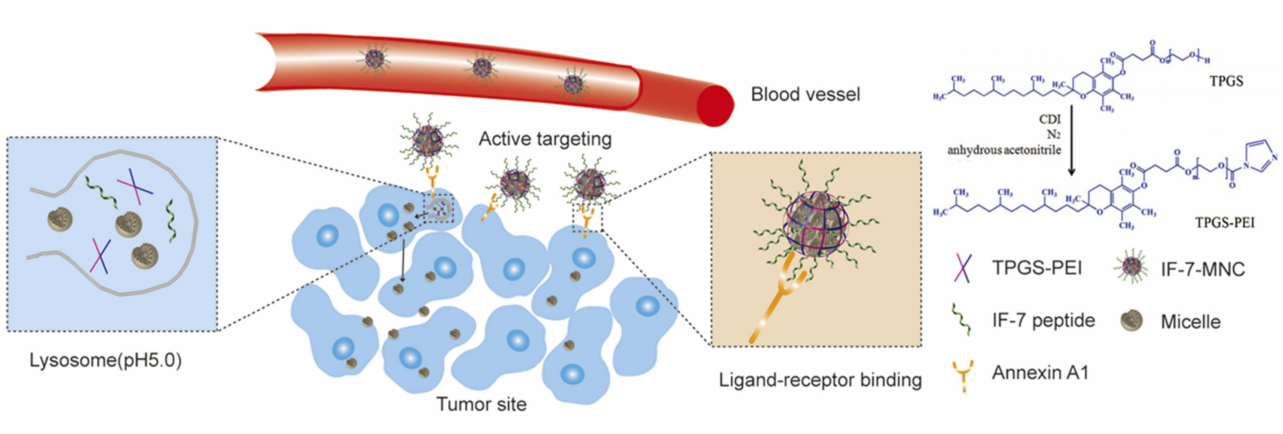

Scheme 1 A carbohydrate mimetic peptide IF-7-modified PEG-PLA/TPGS-PEI micellar nanocluster (IF-7-MNC) was prepared by emulsification–evaporation method to form the cross-link framework of TPGS-PEI to encapsulate the PEG-PLA micelles inside. IF-7 was applied as a targeting motif to bind with receptors in the tumor cells, enhancing IF-7-MNC in vivo chances of tumor accumulation and more micelles released to penetrate into tumor sites.

Biological Technology Co., Ltd. (Shanghai, China). IF-7-Cys-Arg-Arg (MW, 1390.72 Da) was synthesized by GL Biochem Co., Ltd. (Shanghai, China). Coumarin-6 was purchased from Biotium (Hayward, CA, USA). Hoechst 33342 and DAPI were from Beyotime. Biotechnology Co., Ltd. (Nantong, China). Polyethylenimine (PEI; MW, 2000), N,N′-Carbonyldiimidazole (CDI), 1,1-Dioctadecyl-3,3,3,3′-tetramethylindotricarbocyanine iodide (DiR), methyl thiazolyl tetrazolium (MTT), 5-(N, N-Dimethyl) amiloride hydrochloride (DMA), Monensin, NaN3, chlorpromazine hydrochloride, Filipin III, Genistein, and Cytochalasin D were all purchased from Sigma-Aldrich (St. Louis, USA). All other reagents and chemicals were of analytical grade. Dialysis bags (MW, 3500) were provided by Green Bird Technology Co., Ltd. (Shanghai, China) and centrifugal filter devices (MW, 3500) were from Millipore (MA, USA).

Dulbecco's Modified Eagle Medium (DMEM) (high glucose) cell culture medium, Roswell Park Memorial Institute (RPMI) 1640 cell culture medium, 0.25% Trypsin-EDTA, penicillin/streptomycin stock solutions and certified fetal bovine serum (FBS) were all purchased from GIBCO Invitrogen Co. (Carlsbad, USA).

HUVEC and A549 cell lines were purchased from the ATCC (Rockefeller, USA) and were cultured in DMEM and RPMI 1640 medium, respectively, supplemented with 10% FBS and 100 U/mL penicillin under 95% humidity and 5% CO_2 at 37°C.

Male BALB/c mice and nude mice (18–22 g) were supplied by the Experimental Animals Center of Fudan University (Shanghai, China), and were kept under specific pathogen-free conditions. All animal experiments agreed with the guidelines of the ethics committee of Fudan University (Shanghai, China), and were approved by the ethics committee of the School of Pharmacy, Fudan University.

Preparation and characterization of IF-7-MNC

In our previous study, we have successfully synthesized MNC.[23] Briefly, TPGS-CDI was synthesized by activating TPGS with CDI at 40°C for 4 hrs; Blank micelles, micelles loaded with PTX (PM), micelles loaded with Coumarin-6 (CM), and micelles loaded with DiR (DM) were prepared by film-forming method, where these cargos were mixed with PEG–PLA, dissolved in acetonitrile solvents and dried through rotary evaporation. After hydration with deionized water, micelles were formed and filtered through 0.22 μm filters to remove free drug. Afterward, we synthesized MNC and MNC modified with IF-7 (IF-7-MNC) through the emulsification–evaporation method.[31] In brief, 10 mL micelles solutions containing 0.1% PEI were mixed with 20 mg TPGS-CDI dissolved by dichloromethane. After ultrasonication for 30 mins, the solutions were immediately evaporated in rotary at 45°C to remove the residual solvent. Then, the solution with light blue opalescence was filtered through 0.22 μm filters to remove the debris. Afterward, the original nanocluster (MNC-O) was obtained; and then the nanocluster (MNC) was obtained by adding 0.7 mg IgG to MNC-O followed by stirring for 10 mins; while IF-7-MNC was obtained through the same procedure except for replacing IgG with IF-7. IF-7-MNC solution was ultrafiltrated at 4000 rpm for

30 mins to remove the unbinding peptides. PTX-loaded IF-7-MNC (IF-7-PMNC), Coumarin-6-loaded IF-7-MNC (IF-7-CMNC) and DiR-loaded IF-7-MNC (IF-7-DMNC) were fabricated by procedure described above.

The particle size and zeta potential of different nanoclusters were measured through dynamic light scattering (DLS) by using Zeta Sizer Nano series (Malvern Instruments, Worcestershire, UK). The morphology was examined through transmission electron microscopy (TEM; Tecnai G2 Spirit, FEI, Netherlands). The concentrations of different loadings and IF-7 bond to MNC were determined by the system of HPLC, and the drug loading coefficiency (DL) was calculated according to the formula below:

$$DL\% = \frac{\text{amount of drug in micelles}}{\text{amount of the PEG} - \text{PLA and drug}} \times 100\%$$

Evaluation of IF-7-MNC stability in different pH environments

To study the stability of IF-7-MNC against being diluted in various pH levels, PBS (0.01 M, pH 7.4), PBS (0.01 M, pH 6.5), and PBS (0.01 M, pH 5.0) were used to simulate the microenvironment of physiology, tumor, and lysosome, respectively.[32] Thirteen mg/mL IF-7-MNC were diluted with various PBS solutions for several times and incubated for 0.5 hrs at room temperature; afterward, the particle diameters and zeta potential were measured through DLS as described before.

Evaluation of IF-7-PMNC release profile

In vitro release behavior of PMNC and IF-7-PMNC was investigated by the dialysis method.[33] Briefly, 1 mL of PMNC solution or IF-7-PMNC solution (containing 0.2 mg PTX) was added into the pre-swollen dialysis bag (MWCO=3500 Da, Greenbird Inc., Shanghai, China), and then the dialysis bag with a sealed end was submerged fully into 49 mL of acidic buffers (pH 5.0 or 6.5) or PBS (pH 7.4) containing 0.5% Tween 80 to achieve pseudosink conditions. The dialysis was carried out at 37°C at 100 rpm vortex for 24 hrs. The concentration of PTX in samples was analyzed by HPLC with revision for volume replacement. PTX released from PTX stock solution was used as the control.

Cellular-uptake evaluation

A549 and HUVEC were chosen as representative cell lines to evaluate the uptake level of nanoclusters. Two cell lines were seeded in 24-well plates at a density of 1×10^4 per well. After incubation for 24 hrs, the medium was discarded, and cells were incubated in FBS-free RPMI 1640 or DMEM containing CMNC and IF-7-CMNC (100 ng/mL Coumarin-6) for 0.5, 1, 2, and 4 hrs, respectively. Moreover, cells pretreated with IF-7 (4 μg/mL) were then incubated with medium containing IF-7-CMNC, which was used as a control. Finally, the cells were washed with pre-cooled PBS and fixed with 4% paraformaldehyde, followed by visualization under Inverted Fluorescence Microscope (DMI4000D; Leica, Germany).

To quantify the uptake level, cells were treated with the same procedure as described above except for that after incubation with different nanoclusters, the cells were harvested through the treatment of trypsin, and suspended in PBS. The fluorescence intensity was analyzed by Flowcytometry (FACSCalibur; BD, USA).

Evaluation of IF-7-MNC internalization mechanism

To indicate the mechanism of the cell uptake of IF-7-MNC, A549 cells were seed into six-well plates at a density of 1×10^5 cells/well. After incubation for 24 hrs, the medium was discarded, and cells were gently washed with PBS for three times. Then, the cells were pretreated with different endocytosis inhibitors including Chlorpromazine hydrochloride (CPZ;10 μg/mL), Glucose (0.45 M), Filipin III (5 μg/mL), Genistein (0.2 mM), Cytochalasin D (3 μM), Amiloride Hydrochloride (DMA; 10 μM), NaN_3 (1 mg/mL), and Monensin (3 μM). Moreover, 100 μg free peptides IF-7 were also added into A549 cells for pretreatment. Then, IF-7-CMNC (Coumarin-6 100 ng/mL) was added to incubate with cells for 0.5 hrs. Afterward, the cells were washed and suspended in PBS; and the fluorescence intensity was analyzed by Flowcytometry (FACSCalibur; BD, USA).

Evaluation of penetration ability into 3D-tumor spheroids

In order to evaluate the penetration efficacy of IF-7-MNC into 3D-tumor spheroids, the in vitro tumor spheroids were constructed as follows: 150 μL of low melting point agarose containing 2% (w/v) FBS-free 1640 medium was

autoclaved for 30 mins at 121°C in advance, and then quickly added into 48-well plates. After the solution cooled down, 500 μL cell suspensions (1600 cells/mL) were seeded into each well, followed by a gentle shake for 5 mins and incubation at 37°C for 7 days. Afterward, 1640 mediums containing IF-7-CMNC and CMNC were added into respective wells, ensuring the coumarin-6 concentration to reach 200 μg/mL. After 4 hrs incubation, the tumor spheroids were rinsed by pre-cooled PBS for several times and fixed with 4% paraformaldehyde for 0.5 hrs. Then, the tumor spheroids were put in confocal dishes and imaged by a confocal laser scanning microscopy (CLSM710, Leica, Germany).

In vitro cytotoxicity evaluation

To study in vitro cytotoxicity of IF-7-MNC, A549 was chosen as a representative cell line and seeded in a 96-well plate at a density of 5×10^3 cells per well. After incubation for 24 hrs, the medium was removed, and cells were incubated for 96 hrs in DMEM containing PMNC, IF-7-PMNC, and PTX solutions with PTX concentrations ranging from 0.1L to 500 ng/mL. Cells cultured with blank DMEM were used as a control. The cytotoxicity was then measured through MTT assay. Briefly, 200 μL MTT solutions (diluted to 0.5 mg/mL with FBS-free RPMI 1640 or DMEM) were added to each well and the plates were incubated for 4 hrs at 37°C. The supernatants were discarded and 200 μL of dimethyl sulfoxide was added to dissolve the formazan crystal. After incubation for 15 mins at 37°C sheltered from lights, the absorbance at 570 nm was measured by a microplate reader (Synergy 2; Biotek Instruments Inc., USA).

Evaluation of in vivo biodistribution of IF-7-DMNC

In order to study in vivo biodistribution of IF-7-DMNC, we established the model of A549 subcutaneous tumor-bearing nude mice by subcutaneously inoculating 200 μL A549 cell suspensions into the nude mice at a density of 3×10^4 cells/mL. DiR (700–900 nm) was used to label the nanocluster and trace its biodistribution behavior in vivo. After the tumor volume reaching 50–100 mm,[3] DMNC and IF-7-DMNC (1 μg DiR/mice) were intravenously injected into the tumor-bearing mice. Then at 1, 2, 4, 8, 12, and 24 hrs, the nude mice were imaged under an in vivo imaging system (MA, USA). And at the end of the experiment, the mice were sacrificed to harvest organs and tumors for ex vivo imaging.

Evaluation of in vivo anti-tumor efficacy

A549 subcutaneous tumor-bearing nude mice were established by subcutaneously inoculating 200 μL of A549 suspension at a cell density of 2.5×10^4 cells/mL into Balb/C nude mice. When tumor volume reached 50−100 mm^3, the nude mice were divided into four groups (n=6) randomly and administered with saline (as a control), Taxol, PMNC and IF-7- PMNC (10 mg/kg PTX) on days 0, 4, and 8. The tumor volume and body weight were measured every 2 days. Volume of tumors was calculated according to the following formula: Volume = Dmax × $Dmin^2\times0.5$, where Dmax is the longest tumor diameters while Dmin is the shortest (mm). On day 14, mice were sacrificed before the tumors were obtained, weighed, and photographed. The anti-tumor efficacy was characterized through the inhibition rate of tumor (IRT%) which was calculated as follows:

$$\mathrm{IRT}(\%) = \frac{\mathrm{Wc} - \mathrm{Wt}}{\mathrm{Wc}} \times 100\%$$

In the formula, Wc referred to the tumor weight of mice from the control group and Wt referred to that of experiment groups.

Safety evaluation

Subcutaneous tumor-bearing mice were randomly divided into three groups (n=3) and administered with saline (as a control), Taxol, PMNC and IF-7- PMNC (10 mg/kg PTX) on days 0, 4, and 8. Then at the end of the experiment, the treated mice were sacrificed to harvest the main organs (heart, liver, spleen, lung, and kidney) and the blood. The obtained organs were fixed in formalin for H&E staining; and the blood was pre-vortexed for hematology study and hepatorenal evaluation.

Data analysis

Data are presented as mean ± standard deviation (SD), and the difference between groups was analyzed by operating ANOVA for multiple groups and Student's *t*-test for two groups. The difference between two groups was considered statistically significant for $*p<0.05$, $**p<0.01$, and $***p<0.001$.

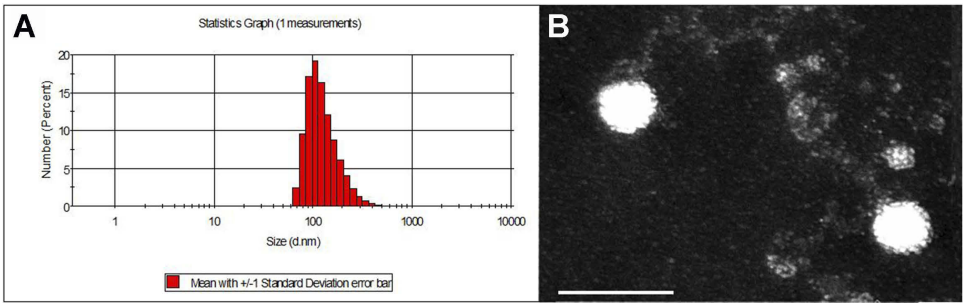

Figure 1 Size distribution (**A**) and TEM image (**B**) of IF-7-MNC. Scale bar =200 nm.
Abbreviation: TEM, transmission electron microscopy.

Results and discussion

Preparation and characterization of IF-7-MNC

Based on the successful synthesis of TPGS-CDI and preparation of micelles as previously reported,[23] IF-7-MNC were successfully prepared and characterized. The results of DSL and TEM are shown in Figure 1. The particle sizes of MNC and IF-7-MNC were 104.2±8.1 and 112.27±6.81 nm, respectively, with polydispersity index <0.2; and the morphology of nanoclusters was clearly observed through TEM, where the micelles were found to be aggregated together. IF-7 could decrease zeta potential of MNC-O from 10.46±2.82 to −4.97 mV ±2.34 mV. Encapsulation of coumarin-6 or PTX did not significantly affect the particle size and zeta potential. According to the HPLC analysis, DL% of IF-7 was 9.41±0.87%.

IF-7 is a strongly negative charged peptide and is qualified to replace IgG to decrease the zeta potential of MNC-O effectively.[34] Considering the poor hydrophilicity of IF-7, we modified the peptide with one cysteine and two arginines to increase the solubility without affecting the properties of IF-7.[35,36] Both the size and zeta potential data indicated that MNC and IF-7-MNC shared the similar physical properties, showing that the replacement of IgG with IF-7 had no impact on the basic chemophysical parameters of nanoclusters.

Furthermore, we have studied the size distribution and morphology of IF-7-MNC after size-shrinkable (Figure S1), and found that IF-7-MNC could disintegrate into independent micelles in acidic environment.

Evaluation of IF-7-MNC pH-responsive characteristic

Two experiments were designed to study pH-responsive characteristics of IF-7-MNC. To be more specific, the stability experiment was used to determine its pH-sensitivity character, while the release profile experiment was used to evaluate the impact of acidic pH environment on the release of PTX from nanoclusters.

The stability study was carried out by using PBS at pH 7.4, 6.5, 5.0 to simulate the microenvironment of physiology, tumor, and lysosome, respectively. IF-7-MNC was diluted from 2 to 100 times; then the size and zeta potential were examined. As shown in Figure 2A, with dilution folds increasing, the particle size of IF-7-MNC in PBS (pH 7.4) stayed about 100 nm without significant fluctuations, and the surface charge gradually decreased to −11.1±2.3 mV, demonstrating that

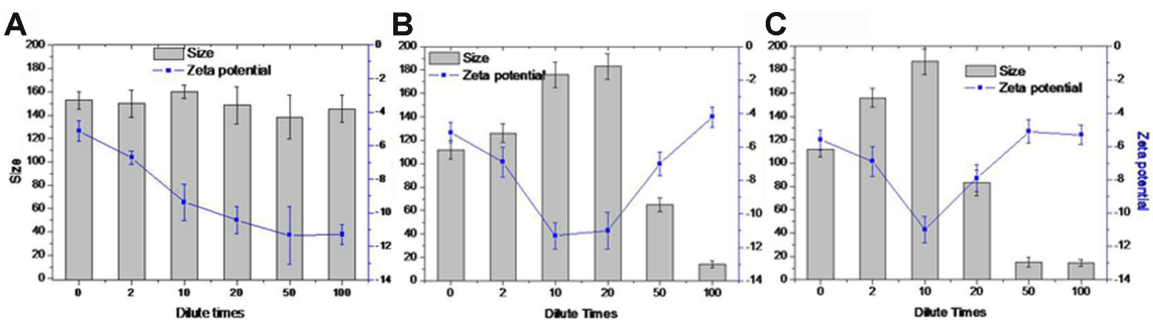

Figure 2 The change of size and zeta potential of IF-7-MNC against dilution by different buffers including (**A**) PBS (pH 7.4), (**B**) PBS (pH 6.5), and (**C**) PBS (pH 5.0).

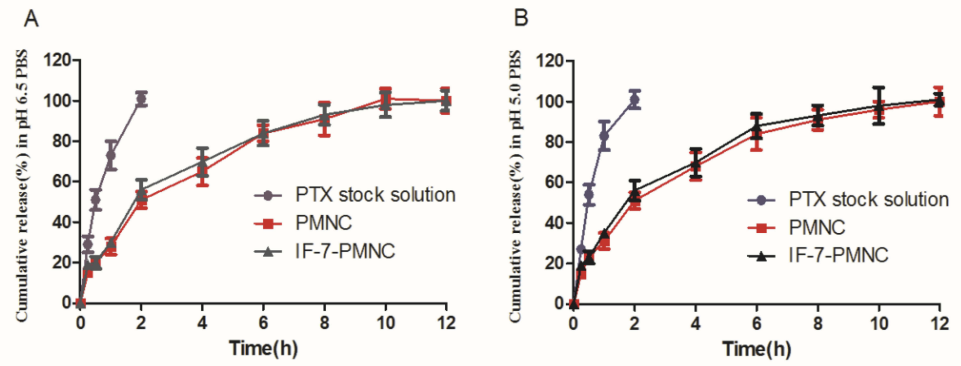

Figure 3 Release profiles of PTX from different PTX formulations in (**A**) PBS (0.01 M, pH 6.5) and (**B**) PBS (0.01 M, pH 5.0) containing 0.5% Tween 80.
Abbreviation: PTX, paclitaxel.

IF-7-MNC had a notable stability against diluting in the physiological pH condition.

On the contrary, the size of IF-7-MNC increased to more than 180 nm when diluted for 20 times (Figure 2B), indicating that IF-7-MNC would dilate to some degree in the acid environment. When the dilution times increased to 50 folds, IF-7-MNC shrunk sharply to nearly 70 nm and finally stabilized at around 15 nm. The results indicated that IF-7-MNC could shift to the size of micelles in an acidic environment like tumor microenvironment. The similar phenomenon was also observed in PBS (0.01 M, 5.0) (shown in Figure 2C), illustrating that size-shrinkable could also be achieved in the acidic environment of lysosome, which would facilitate the intracellular drug release of IF-7-MNC.

To further prove the pH-responsive trait of IF-7-MNC, the release profile evaluation was carried out by dialysis method. The release of PTX-loaded IF-7-MNC and MNC were examined at two different pH values: PBS (0.01 M, pH 6.5) medium was used for mimicking the tumor environment and PBS (0.01 M, pH 5.0) medium was for lysosomal acidity.[37] As shown in Figure 3, the pH of PBS had no influence on the release of PTX from the stock solution, since more than 99% PTX could freely diffuse through dialysis membrane within the first 2 hrs. However, in acidic solutions, the cumulative release of PTX from both PMNC and IF-7-PMNC was achieved in 12 hrs, which displayed a slow-release profile of the drug-loaded nanoclusters, confirming the pH-sensitivity of MNC.

When the nanoclusters were present in an acid environment, a large number of protons would be captured by the unsaturated amino groups of PEI, resulting in the inflow of H_2O and Cl^-, during which the process was similar to that of nanogels.[38] Accordingly, MNC would expand to larger size. The influx of H_2O and Cl^- would gradually increase the inner osmotic pressure of the nanocluster, which might be balanced with elasticity of the polymer in framework.[39] Since it has reported that the swelling extent of nanoparticles was attributed to the balance between the polymer elasticity and interior osmotic pressure.[40] In the system of MNC, TPGS cross-linked with PEI through a single end linkage, which indicated that with the increase of osmotic pressure, the plasticity of the cross-linked structure was not durable enough to balance the inner pressure. Consequently, once the swelling extent reached a certain degree, TPGS-PEI structure could be disintegrated.

Evaluation of IF-7-MNC cellular-uptake level and internalization mechanism

Figure 4A displays the qualitative results of various MNC preparations taken in by A549 cells. The green fluorescence indicated the internalized CMNC or IF-7-CMNC, and the fluorescent intensity was the reflection of cellular-uptake level. The internalization level of these three formulations showed a time-dependent manner: as the time of incubation prolonged, the fluorescence intensity of each group was gradually increased and reached at the maximum value at 2 hrs. Moreover, at each time point, the cellular-uptake level of IF-7-CMNC was more significant than that of CMNC by A549, indicating that IF-7 receptor binding with Annexin1 expressed in A549 cells favored the uptake of MNC. And the qualitative results (shown in Figure 4B) analyzed via the flow cytometry were consistent with quantitative results. Nevertheless, the internalization level of IF-7-CMNC was significantly reduced in A549 pretreated with IF-7 polypeptide, which could be due to that the free IF-7 polypeptide initially bond with

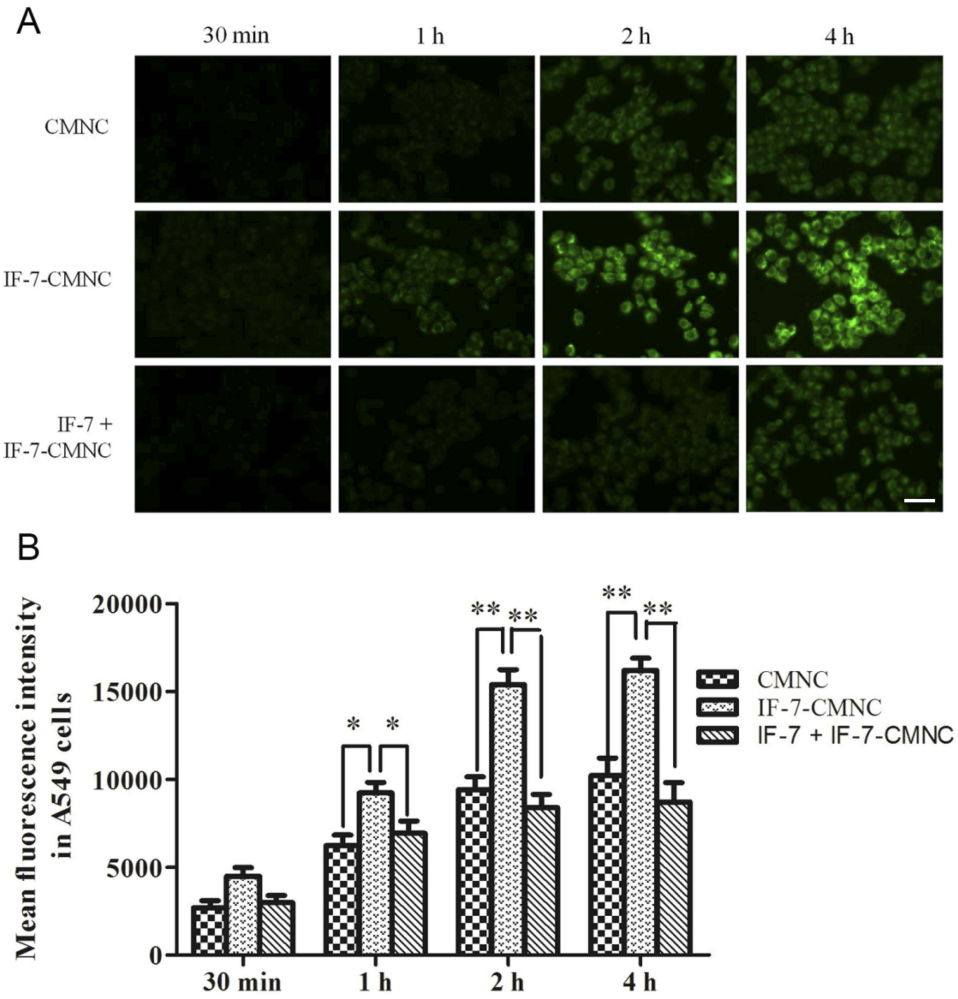

Figure 4 Qualitative and quantitative results of CMNC and IF-7-CMNC taken in by A549 cells. Cells pre-incubated with 100 μg IF-7 was served as control. (**A**) The cellular-uptake level of IF-7-CMNC by A549 cells was imaged at 0.5, 1, 2, and 4 hrs. Scale bar =100 μm. (**B**) The quantitative results of CMNC and IF-7-CMNC taken in by A549 cells analyzed by flow cytometry. (n=3). *p<0.05, **p<0.01.

Annexin 1 on the surface of A549. The competitive inhibition was caused by the pre-binding of Annexin 1 with free IF-7 peptides, which reduced the accessible Annexin 1 receptors for specific recognition and therefore impeded the internalization pathway of IF-7-CMNC initiated by Annexin 1-IF-7 binding. This also proved that IF-7 played a major role as the targeting motif of A549 cell uptake. Moreover, we chose HUVEC cell line where Annexin 1 is also highly expressed as another in vitro model to evaluate the cellular-uptake level of IF-7-CMNC, and the results shown in Figure S2 were consistent with the result above.

Furthermore, we have studied the internalization mechanism of IF-7-MNC. It is known that there are three endocytic pathways: caveolae-mediated endocytosis, clathrin-mediated endocytosis, and micropinocytosis.[41] In order to reveal the internalization mechanism of IF-7-MNC in A549 cells, we pre-incubated various endocytosis inhibitors and free IF-7 polypeptides with A549 cells before IF-7-MNC incubation. Inhibitors used for this study were listed as follows: CPZ and Glucose were clathrin-mediated endocytosis inhibitors; Cytochalasin D Filipin and Genistein were caveolae-mediated endocytosis inhibitors; and DMA could inhibit micropinocytosis; NaN_3 was an energy-depletion agent; Monensin was a lysosome inhibitor. We perceived from Figure S3 that the inhibitors of three endocytosis pathways were all able to limit the internalization efficiency of IF-7-MNC in A549 cells, and energy-depletion by NaN_3 also restrained the cellular uptake of the nanocluster by A549 cells. The internalization could also be inhibited significantly by Monensin (p<0.05), which indicated that IF-7-MNC would go through the lysosome. Moreover, free IF-7 polypeptides could restrict almost 45% of IF-7-MNC to be taken by A549, which was consistent with the findings of cellular-internalization study before. As it is known that the receptor-

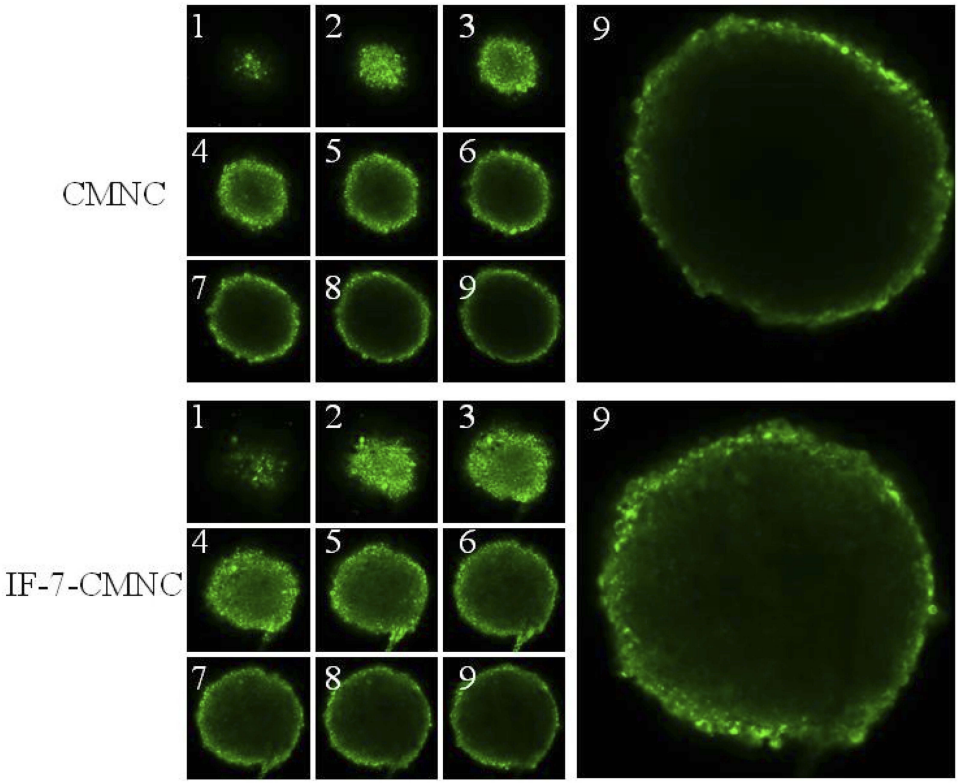

Figure 5 CMNC and IF-7-CMNC penetrated into tumor spheroids after 4 hrs incubation with the 100 ng/mL of Coumarin-6. Multi-level scan interval: 10 μm.

mediated endocytosis is generally inhibited when the specific ligands exist excessively,[42] the result could be explained as the excessive IF-7 peptides bond with AnnA1 before the IF-7-MNC internalization, reducing the AnnA1 receptors available for binding mediated with IF-7.

Evaluation of IF–MNC penetration ability into tumor spheroids

The 3D-tumor spheroids were constructed to mimic the pathologic characteristics of solid tumor, which might simulate in vivo tumor cell density, cell-matrix, hypoxia, and other biofeatures.[43] Hence, A549 tumor spheroids were employed to study the penetrating efficiency of these nanoclusters labeled with coumarin-6. As shown in Figure 5, with the same scan depth, ie 90 μm, the tumor spheroid incubated with IF-7-CMNC displayed stronger green fluorescence intensity than that with CMNC, indicating IF-7-CMNC had a stronger ability to penetrate tumor spheroids than CMNC. It has been proved in our previous study that the nanocluster could be disintegrated in the lysosome and released the micelles inside to escape from the cells, and then penetrated into the cell interstitial.[23] Here, with the same penetration depth, more extensive distribution of IF-7-MNC might be attributed to that IF-7 benefitted the internalization of IF-7-CMNC through the specific binding with AnnA1.

In vivo biodistribution study

As shown in Figure 6A, with the blood circulation time prolonged, the fluorescence of IF-7-DMNC gradually increased at the tumor sites and reach maximum at 24 hrs. The semi-quantitative results shown in Figure 6B displayed that after i.v. administration for 4 hrs, the in vivo fluorescent intensity of IF-7-DMNC at the tumor site was higher than that of DMNC at each experimental point. On the other hand, DMNC were more distributed in the liver; and at 24 hrs, the main organs and tumors were harvested for ex vivo imaging and quantification, and the quantitative results shown in Figure 6C illustrated that the fluorescence intensity of IF-7-DMNC in the tumor was about 4.5-fold stronger than that of DMNC, while the fluorescence intensity of IF-7-DMNC amount to 69.4% and 53.4% of DMNC in the liver and the spleen, respectively. These results proved that compared with DMNC which accumulated toward the subcutaneous tumor

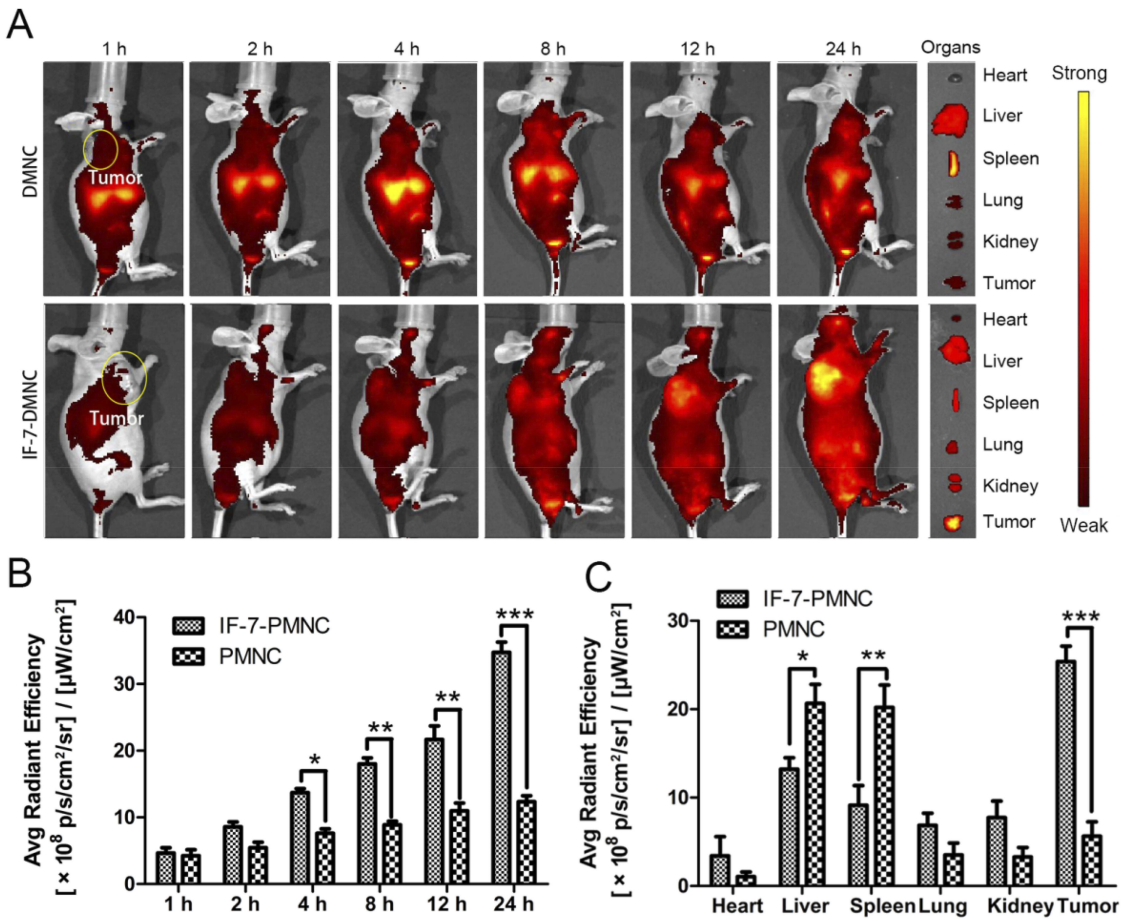

Figure 6 In vivo tumor-targeting efficacy evaluation of DMNC and IF-7-DMNC. (**A**) Living imaging of A549 subcutaneous tumor-bearing nude intravenously injected with Coumarin-labeled nanoclusters at 1, 2, 4, 8, 12, and 24 hrs, respectively. (**B, C**) Quantitative results of in vivo and ex vivo imaging.

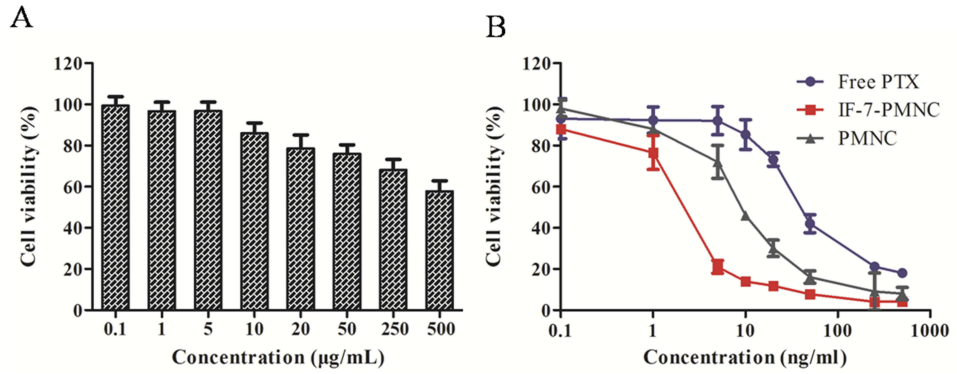

Figure 7 A549 cell viability evaluation. (**A**) Viability of A549 cells treated with various concentrations of blank IF-7-MNC; (**B**) viability of A549 cells treated with various PTX formulations, including free PTX, PMNC, and IF-7-PMNC (n=6).

through a passive targeting way, IF-7-DMNC exhibited a prominent active tumor-targeting ability and effectively avoided the clearance effect by RES. There have been some studies reporting that polyamino acids or "self" peptides could modify the surface of nanoparticles to reduce the in vivo clearance mediated by macrophages.[44] Herein, IF-7 could lead to less phagocytosis of MNC by macrophages and more specific target to the tumor site by AnnA1 recognition.

In vitro cytotoxicity evaluation

As displayed in Figure 7A, after incubation for 96 hrs, the cytotoxicity of the blank MNC was negligible at

Table 1 IC_{50} of different PTX formulations on A549 cells (n=6)

Formulation	IC_{50} (ng/mL)
Free PTX	52.37±7.51
PMNC	9.68±2.20**
IF-7-PMNC	2.17±0.76***

Notes: **p<0.01, ***p<0.001, significantly different from free PTX.
Abbreviation: PTX, paclitaxel.

concentrations ranging from 0.1 to 500 μg/mL. The cytotoxicity increased slightly as the concentration enhanced, while the IC_{50} value of IF-7-MNC against A549 cells was still larger than 500 μg/mL, confirming that the nanocluster had no significant toxicity on A549 viability hence could be safely used to deliver PTX.

As shown in Figure 7B, with PTX concentrations varying from 0.1 to 1000 ng/mL, the most significant reduction in the A549 cell viability was found in the group incubated with IF-7-PMNC. And the IC_{50} values after incubation for 96 hrs with different PTX formulations are compared in Table 1: IF-7-PMNC < PMNC < Free PTX. To be more specific, the IC_{50} value of free PTX against A549 cells was 5.4-fold and 24.1-fold higher than that of PMNC and IF-7-PMNC, respectively. And the significant difference between PMNC and IF-7-PMNC (p<0.01) showed that PMNC group had a notably greater cytotoxic effect on A549 cells, which might be due to the enhanced uptake of nanoclusters by A549 cells.

In vivo anti-tumor efficacy

As shown in the curve of tumor growth in Figure 8A, compared with the control group treated with saline, the tumor growth of IF-7-PMNC treated group and PMNC treated groups were both significantly inhibited. Wherein, IF-7-PMNC showed a stronger inhibition effect on the tumor growth than that of PMNC. Especially during the first 4 days after administration, the tumor volume of the IF-7-PMNC group increased much more slowly than that of other groups. The change of body weight was shown in Figure 8B, indicating that compared with the control group, there were only minor changes of body weight in the two

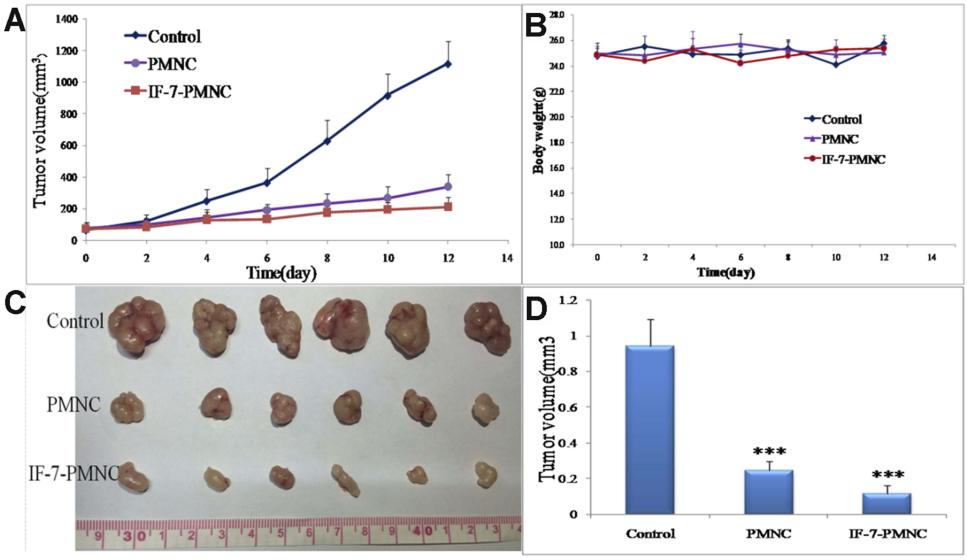

Figure 8 Anti-tumor growth efficacy of different PTX formulations in A549 subcutaneous tumor-bearing nude mice (n=6). (**A**) Tumor volumes and (**B**) body weight of nude mice changed with time elapsed. (**C**) Tumor size and morphology at the experimental end point (12th day). (**D**) Tumor weight at the experimental end point (12th day). ***p<0.001.

Table 2 Anti-tumor effects of PTX formulations against A549 subcutaneous tumor in Balb/c mice (n=6)

Groups	Dose (mg/kg)	Body weight (g)		Related tumor weight	IRT (%)
		Initial	Final		
Control	–	24.82±1.29	25.89±1.34	0.94±0.14	–
PMNC	10	24.69±1.67	25.44±1.30	0.25±0.05	73.40
IF-7-PMNC	10	24.49±1.52	25.56±0.99	0.11±0.04	88.29*

Notes: *p<0.05, significantly different with PMNC group.

different MNC groups and basically maintained at about 25 g, proving that MNC preparation carrier groups had low toxicity to the body. On 12 days after administration, mice were sacrificed, and the tumors were obtained for photographing (shown in Figure 8C), and the tumor weight of each group was quantified in Figure 8D. The inhibition rate of tumor weight was calculated and shown in Table 2, demonstrating that PMNC and IF-7-PMNC both played an inhibitory role in tumor growth, while PMNC modified with IF-7 could increase the inhibitory rate from 73.40% to 88.29% ($p<0.05$).

The in vivo anti-tumor result demonstrated that the tumor growth-inhibiting efficacy was determined more than the cytotoxicity of chemotherapeutics but also the amounts accumulated at the tumor site and penetrated into the inner part. IF-7-PMNC enhanced the chemotherapeutics accumulation via ligand-receptor recognition when compared with PMNC accumulated through EPR effects. Since the chances of nanocluster enriching at the tumor sites could be improved by Annexin 1-IF-7 binding, the amounts of micelles escaped from the lysosome and penetrated through the tumor interior could also be increased. According to all these results, IF-7-PMNC would outperform other formulations and exhibited the most extraordinary suppressive effect on tumor development.

Moreover, there have been some studies reporting that the polymeric micelles could be used to treat multidrug-resistant tumors,[45,46] which inspires us to update the biomaterials with curative functions for our micelle nanocluster, furthering its therapeutic application in cancer treatment.

In vivo safety evaluation

The in vivo toxicity of different nanocluster was studied. As shown in Figure 9, no obvious pathological damage was found in the main organs (heart, liver, spleen, lung, and kidney). And the hematology study showed compared with the group treated with saline, no significant differences were counted in the number of white blood cells, red blood cells, and platelets of MNC and IF-7-MNC groups (displayed in Table 3).

Conclusion

In this study, IF-7-modified size-shrinkable MNC (IF-7-MNC) was constructed via binding IF-7 to the surface of

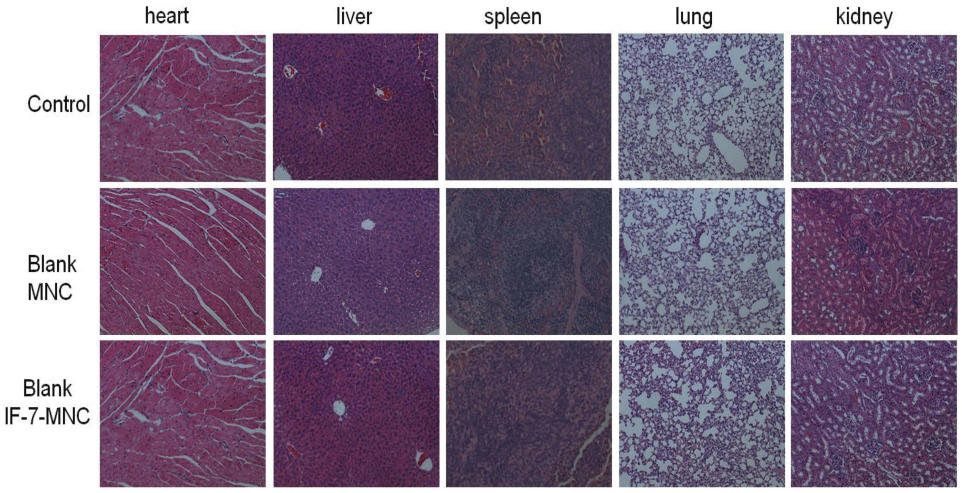

Figure 9 H&E stained heart, liver, spleen, lung, and kidney sections isolated from A549 subcutaneous tumor-bearing nude mice after treatment with saline, blank MNC and blank IF-7-MNC every 4 days 1 for three continuous times. Images were obtained by using a Lesica microscope. Original magnification: 20×.

Table 3 Blood cell counts of nude mice after treatments with saline, MNC, and IF-7-MNC (n=3)

Group	WBC (10^9cells/L)	RBC(10^{12} cells/L)	Platelets(10^9 cells/L)
Saline	5.02±0.88	10.81±1.67	1309±310.2
MNC	5.41±1.19	10.62±1.22	1393±211.8
IF-7-MNC	5.06±0.95	9.96±0.73	1336±194.4

the pH-sensitive and cross-linked structure through the electrostatic adsorption, with micelles aggregated inside the framework. The particle size was 112.27±6.81 nm and the morphology examined by TEM displayed the delivery system in the form of MNC. The distending of IF-7-MNC could happen when it was present in the acid conditions, and the structure could slowdown the release of PTX loaded in the micelles. Moreover, compared with MNC, in vitro evaluations showed that IF-7-MNC could be more significantly internalized into A549 cells and HUVEC cells, as well as with a stronger penetration efficacy into the 3D-tumor spheroids. The biodistribution study has shown that IF-7-MNC could more accumulated at the tumor sites, exhibiting better tumor-targeting capability. The in vivo anti-tumor results also showed a prominent inhibitory effect on tumor growth of IF-7-MNC. The safety evaluation proved it was of lower toxicity to be used in vivo. In conclusion, IF-7-modified size-shrinkable MNC was of great application potential in cancer therapy.

Acknowledgment

The authors acknowledge the financial support from the National Natural Science Foundation of China (81773201), Fudan-SIMM Joint Research Fund (FU-SIMM20182005), PDH-SPFDU Joint Research Fund (RHJJ2018-02), Development Project of Shanghai Peak Disciplines-Integrative Medicine (20180101), and the flexible talent program in Xinjiang province, China.

Disclosure

The authors report no conflicts of interest. The authors alone are responsible for the content and writing of this article.

References

1. Caragher SP, Sachdev S, Ahmed AU. Radiotherapy and glioma stem cells: searching for chinks in cellular armor. *Curr Stem Cell Rep*. 2017;3(4):348–357. doi:10.1007/s40778-017-0102-8
2. Singh RK, Singh DP, Tiwari SP, et al. Targeted therapies for cancer treatment. *J Pharm Res*. 2011;4(2):312–316.
3. Chen M, Lin Z, Ling M. Near-infrared light-activatable microneedle system for treating superficial tumors by combination of chemotherapy and photothermal therapy. *ACS Nano*. 2015;10(1):93–101. doi:10.1021/acsnano.5b05043
4. Block JB. Cancer chemotherapy reports. *CA Cancer J Clin*. 2010;23(3):182–183.
5. Steward LT, Gao F, Taylor MA, Margenthaler JA. Impact of radiation therapy on survival in patients with triple-negative breast cancer. *Oncol Lett*. 2014;7(2):548–552. doi:10.3892/ol.2013.1700
6. Imai E. Gene therapy for renal diseases: its potential and limitation. *J Am Soc Nephrol*. 2003;14(4):1102–1104. doi:10.1097/01.asn.0000067655.48829.d5
7. Urbina JA. Specific chemotherapy of Chagas disease: relevance, current limitations and new approaches. *Acta Trop*. 2010;115(1–2):55–68. doi:10.1016/j.actatropica.2009.10.023
8. Nguyen KT. Targeted nanoparticles for cancer therapy: promises and challenges. *J Nanomed Nanotechnol*. 2011;2(5). doi:10.4172/2157-7439.1000103e
9. Torchilin VP. Targeted polymeric micelles for delivery of poorly soluble drugs. *Cell Mol Life Sci*. 2004;61(19–20):2549–2559. doi:10.1007/s00018-004-4153-5
10. Tanford C. Micelle shape and size. *J Phys Chem*. 1972;76(21):3020–3024. doi:10.1021/j100665a018
11. Rapoport N. Drug delivery in polymeric micelles: from in vitro to in vivo. *J Control Release*. 2003;91(1–2):85–95.
12. Kim SC, Kim DW, Shim YH, et al. In vivo evaluation of polymeric micellar paclitaxel formulation: toxicity and efficacy. *J Control Release*. 2001;72(1–3):191–202.
13. Sun X, Wang G, Zhang H, et al. The blood clearance kinetics and pathway of polymeric micelles in cancer drug delivery. *ACS Nano*. 2018;12(6):6179–6192. doi:10.1021/acsnano.8b02830
14. Le Garrec D, Gori S, Luo L, et al. Poly(N-vinylpyrrolidone)-block-poly(d,l-lactide) as a new polymeric solubilizer for hydrophobic anticancer drugs: in vitro and in vivo evaluation. *J Control Release*. 2004;99(1):83–101. doi:10.1016/j.jconrel.2004.06.018
15. Muley P, Kumar S, El Kourati F, Kesharwani SS, Tummala H. Hydrophobically modified inulin as an amphiphilic carbohydrate polymer for micellar delivery of paclitaxel for intravenous route. *Int J Pharmaceut*. 2016;500(1–2):32–41. doi:10.1016/j.ijpharm.2016.01.005
16. Jain RK, Stylianopoulos T. Delivering nanomedicine to solid tumors. *Nat Rev Clin Oncol*. 2010;7(11):653–664. doi:10.1038/nrclinonc.2010.139
17. Fang J, Nakamura H, Maeda H. The EPR effect: unique features of tumor blood vessels for drug delivery, factors involved, and limitations and augmentation of the effect. *Adv Drug Deliver Rev*. 2011;63(3):136–151. doi:10.1016/j.addr.2010.04.009
18. Maeda H, Bharate GY, Daruwalla J. Polymeric drugs for efficient tumor-targeted drug delivery based on EPR-effect. *Eur J Pharm Biopharm*. 2009;71(3):409–419. doi:10.1016/j.ejpb.2008.11.010
19. Perrault SD, Walkey C, Jennings T, Fischer HC, Chan WCW. Mediating tumor targeting efficiency of nanoparticles through design. *Nano Lett*. 2009;9(5):1909–1915. doi:10.1021/nl900031y
20. Stirland DL, Nichols JW, Miura S, Bae YH. Mind the gap: a survey of how cancer drug carriers are susceptible to the gap between research and practice. *J Control Release*. 2013;172(3):1045–1064. doi:10.1016/j.jconrel.2013.09.026
21. Danhier F. To exploit the tumor microenvironment: since the EPR effect fails in the clinic, what is the future of nanomedicine? *J Control Release*. 2016;244:108–121. doi:10.1016/j.jconrel.2016.11.015
22. Nichols JW, Bae YH. EPR: evidence and fallacy. *J Control Release*. 2014;190:451–464. doi:10.1016/j.jconrel.2014.03.057
23. Jain RK, McKee T, Pluen A, et al. Dynamic imaging of collagen and its modulation in tumors in vivo using second-harmonic generation. *Nat Med*. 2003;9(6):796–800. doi:10.1038/nm879
24. Liang H, Ren X, Qian J, et al. Size-shifting micelle nanoclusters based on a cross-linked and pH-sensitive framework for enhanced tumor targeting and deep penetration features. *Acs Appl Mater Inter*. 2016;8(16):10136–10146. doi:10.1021/acsami.6b00668
25. Shingo H, Kazuhiro S, Shibata TK, et al. Targeted drug delivery to tumor vasculature by a carbohydrate mimetic peptide. *Proc Natl Acad Sci U S A*. 2011;108(49):19587–19592. doi:10.1073/pnas.1105057108
26. Gerke V, Creutz CE, Moss SE. Annexins: linking Ca2+ signalling to membrane dynamics. *Nat Rev Mol Cell Bio*. 2005;6(6):449–461. doi:10.1038/nrm1661
27. Tsu-Yao C, Ming-Shiang W, Jaw-Town L, et al. Annexin A1 is associated with gastric cancer survival and promotes gastric cancer cell invasiveness through the formyl peptide receptor/extracellular signal-regulated kinase/integrin beta-1-binding protein 1 pathway. *Cancer Am Cancer Soc*. 2012;118(23):5757.

28. de Graauw M, van Miltenburg MH, Schmidt MK, et al. Annexin A1 regulates TGF- signaling and promotes metastasis formation of basal-like breast cancer cells. *Proc Natl Acad Sci*. 2010;107(14):6340–6345. doi:10.1073/pnas.0913360107
29. Neri D, Bicknell R. Tumour vascular targeting. *Nat Rev Cancer*. 2005;5(6):436–446. doi:10.1038/nrc1627
30. Simon MA, Enrico C, Mario P, et al. Annexin A1: a central player in the anti-inflammatory and neuroprotective role of microglia. *J Immunol*. 2010;185(10):6317–6328. doi:10.4049/jimmunol.1001095
31. Vinogradov SV, Bronich TK, Kabanov AV. Nanosized cationic hydrogels for drug delivery: preparation, properties and interactions with cells. *Adv Drug Deliv Res*. 2002;54(1):135–147. doi:10.1016/S0169-409X(01)00245-9
32. Peisheng X, Kirk EAV, Yihong Z, Murdoch WJ, Maciej R, Youqing S. Targeted charge-reversal nanoparticles for nuclear drug delivery. *Angew Chem Int Edit*. 2010;46(26):4999–5002.
33. D'Souza SS, Deluca PP. Development of a dialysis in vitro release method for biodegradable microspheres. *AAPS PharmSciTech*. 2005;6(2):E323–E328. doi:10.1208/pt060242
34. Yu DH, Liu YR, Luan X, et al. IF7-conjugated nanoparticles target Annexin 1 of tumor vasculature against P-gp mediated multidrug resistance. *Bioconjugate Chem*. 2015;26(8):1702. doi:10.1021/acs.bioconjchem.5b00283
35. Arakawa T, Kita Y, Koyama AH. Solubility enhancement of gluten and organic compounds by arginine. *Int J Pharm*. 2008;355(1):220–223. doi:10.1016/j.ijpharm.2007.12.009
36. Tripathi M, Kohli DV, Uppadhyay RK. Enhancement of solubility and dissolution of indomethacin and phenylbutazone by cholic and deoxycholic acid conjugates. *Drug Dev Commun*. 2008;18(1):135–141.
37. Yangyang Z. Qingyan, et al. Ratiometric fluorescent detection of acidic pH in lysosome with carbon nanodots. *Chin Chem*. 2017;28(10):1969–1974. doi:10.1016/j.cclet.2017.07.027
38. Raemdonck K, Demeester J, De Smedt S. Advanced nanogel engineering for drug delivery. *Soft Matter*. 2009;5(4):707–715. doi:10.1039/B811923F
39. Tu ZC, Ge LQ, Li JB, Ou-Yang ZC. Elasticity of polymer vesicles by osmotic pressure: an intermediate theory between fluid membranes and solid shells. *Phys Rev E*. 2005;72(2):21806. doi:10.1103/PhysRevE.72.021806
40. Hedrick MM, Jun Kyung C, Denton AR. Structure and osmotic pressure of ionic microgel dispersions. *J Chem Phys*. 2015;142(3):511–931. doi:10.1063/1.4905574
41. Bhattacharyya S, Mulherkar N, Chandran K. Endocytic pathways involved in filovirus entry: advances, implications and future directions. *Viruses*. 2012;4(12):3647–3664.
42. Nunes R, Kiang CL, Sorrentino D, Berk PD. Albumin-receptor' uptake kinetics do not require an intact lobular architecture and are not specific for albumin. *J Hepatol*. 1988;7(3):293. doi:10.1016/S0168-8278(88)80001-1
43. Geeta M, Hsiao AY, Marylou I, Luker GD, Shuichi T. Opportunities and challenges for use of tumor spheroids as models to test drug delivery and efficacy. *J Control Release*. 2012;164(2):192–204. doi:10.1016/j.jconrel.2012.04.045
44. Tianjiao J, Yanping D, Ying Z, et al. Peptide assembly integration of fibroblast-targeting and cell-penetration features for enhanced anti-tumor drug delivery. *Adv Mater*. 2015;27(11):1865–1873. doi:10.1002/adma.201404715
45. Kesharwani SS, Kaur S, Tummala H, Sangamwar AT. Multifunctional approaches utilizing polymeric micelles to circumvent multidrug resistant tumors. *Colloids Surf B*. 2018;1(173):581–590.
46. Kesharwani SS, Kaur S, Tummala H, Sangamwar AT. Overcoming multiple drug resistance in cancer using polymeric micelles. *Expert Opin Drug Deliv*. 2018;11(15):1127–1142. doi:10.1080/17425247.2018.1537261